(12) B.S. LEVEL II

DNA 5265F

PROPAGATION MODELING AND EVALUATION OF COMMUNICATION SYSTEM PERFORMANCE IN NUCLEAR ENVIRONMENTS

Charles L. Rino

SRI International
333 Ravenswood Avenue
Menlo Park, California 94025

29 February 1980

Final Report for Period 11 November 1976—29 February 1980

CONTRACT No. DNA 001-77-C-0038

THIS WORK SPONSORED BY THE DEFENSE NUCLEAR AGENCY
UNDER RDT&E RMSS CODE B322078464 S99QAXHB05415 H2590D.

Prepared for
Director
DEFENSE NUCLEAR AGENCY
Washington, D. C. 20305

Destroy this report when it is no longer needed. Do not return to sender.

PLEASE NOTIFY THE DEFENSE NUCLEAR AGENCY, ATTN: STTI, WASHINGTON, D.C. 20305, IF YOUR ADDRESS IS INCORRECT, IF YOU WISH TO BE DELETED FROM THE DISTRIBUTION LIST, OR IF THE ADDRESSEE IS NO LONGER EMPLOYED BY YOUR ORGANIZATION.

(18) DNA, SBIE

UNCLASSIFIED

SECURITY CLASSIFICATION OF THIS PAGE (When Data Entered)

(19) **REPORT DOCUMENTATION PAGE**

READ INSTRUCTIONS BEFORE COMPLETING FORM

1. REPORT NUMBER: DNA 5265F, AD-E300 890 / 2. GOVT ACCESSION NO: AD-A088914	3. RECIPIENT'S CATALOG NUMBER
4. TITLE (and Subtitle): (6) PROPAGATION MODELING AND EVALUATION OF COMMUNICATION SYSTEM PERFORMANCE IN NUCLEAR ENVIRONMENTS.	5. TYPE OF REPORT & PERIOD COVERED: (9) Final Report, 11 Nov 76—29 Feb 80
	6. PERFORMING ORG. REPORT NUMBER: SRI Project 5960
7. AUTHOR(s): (10) Charles L. Rino	8. CONTRACT OR GRANT NUMBER(s): (15) Contract DNA 001-77-C-0038
9. PERFORMING ORGANIZATION NAME AND ADDRESS: SRI International, 333 Ravenswood Avenue, Menlo Park, California 94025	10. PROGRAM ELEMENT, PROJECT, TASK AREA & WORK UNIT NUMBERS: (16) Subtask S99QAXHB054-15
11. CONTROLLING OFFICE NAME AND ADDRESS: Director, Defense Nuclear Agency, Washington, D.C. 20305	12. REPORT DATE: 29 Feb 1980 / 13. NUMBER OF PAGES: 44
14. MONITORING AGENCY NAME & ADDRESS (if different from Controlling Office): (17) B054 (12) 43	15. SECURITY CLASS (of this report): UNCLASSIFIED / 15a. DECLASSIFICATION/DOWNGRADING SCHEDULE

16. DISTRIBUTION STATEMENT (of this Report)

Approved for public release; distribution unlimited.

17. DISTRIBUTION STATEMENT (of the abstract entered in Block 20, if different from Report)

18. SUPPLEMENTARY NOTES

This work sponsored by the Defense Nuclear Agency under RDT&E RMSS Code B322078464 S99QAXHB05415 H2590D.

19. KEY WORDS (Continue on reverse side if necessary and identify by block number)

Binary Communication
Channel Model
Error Rate
Power Law
Scintillation

20. ABSTRACT (Continue on reverse side if necessary and identify by block number)

This report summarizes propagation modeling work for predicting communication-system performance in disturbed nuclear environments. Simple formulas are developed that characterize the onset of scintillation, the coherence time of the scintillation, the coherence bandwidth loss and associated delay jitter, plus the angle-of-arrival scintillation for radar applications. The calculations are based on a power-law phase-screen model, and they fully accommodate a varying spectral index and arbitrary propagation angles relative to the

DD FORM 1 JAN 73 1473 EDITION OF 1 NOV 65 IS OBSOLETE

UNCLASSIFIED

SECURITY CLASSIFICATION OF THIS PAGE (When Data Entered)

410281

20. ABSTRACT (Continued)

principal irregularity axis. In a power-law environment, the signal structure is critically dependent upon the power-law index, particularly under strong-scatter conditions.

CONTENTS

ILLUSTRATIONS

I EXECUTIVE SUMMARY

This report completes the propagation modeling work performed under DNA Contract DNA001-77-C-0038 (SRI Project 5960). The broad objective of this work was to develop a unifying theoretical framework for the various nuclear-propagation predictions based on (1) numerical simulations, (2) field measurements, using the naturally and artificially disturbed ionosphere, and (3) predictive computer codes for systems analysis.

It is now generally accepted that knowledge of the striation spectral-density function (SDF) suffices for predicting the signal moments that characterize the average disturbed-signal structure. The mathematical form of the SDF follows a power law. The range of the power-law continuum and the appropriate spectral index, however, admit some uncertainties.

Naturally occurring phase scintillation admits a power-law spectral characterization over a scale-size range from tens of kilometers to hundreds of meters with a one-dimensional power-law index near 2.5. For typical barium releases, the power-law continuum evidently does not extend to scale sizes larger than one kilometer. The corresponding phase spectrum, derived from back-propagated LES-8 signals during the STRESS experiments, gives a power-law index somewhat greater than three [Knepp and Bogusch, 1979]. These results are not necessarily in conflict, but they do imply that the propagation theory must accommodate some variation in spectral slope.

The theoretical work performed under this contract fully accommodates a varying spectral index. The results show that the signal structure in a power-law environment is critically dependent on the power-law slope, particularly under strong-scatter conditions. The effects are subtle, but they do affect predictive modeling.

The predictive modeling problem is typically broken into two parts. The weak-scatter theory is linearly extrapolated to determine the onset of saturated scintillation. The Rayleigh model, which is completely characterized by the mutual coherence function, is then assumed to apply. This scheme is generally adequate. Our work shows, however, that in a power-law environment the Rayleigh limiting form can only be strictly achieved when the phase spectral index is less than 3, as is evidently the case for naturally occurring scintillation.

It is intended that this report be self contained; thus, some background material is presented in Section II. In Section III we summarize the weak-scatter theory that characterizes the onset of amplitude and phase scintillation. A detailed development can be found in Rino (1979a). In Section IV the general formulas for the phase-screen model are developed. The general formulation fully allows for wavefront curvature, which was not explicitly included in our previous calculations based on incident plane waves. The spherical-wave correction factors are easily applied to the previously developed plane-wave results.

In Section V a model for the mutual-coherence function is developed and then used to derive simple formulas for the signal-coherence times. Two approximations are used: one valid for shallowly sloped spectra; the other for the more steeply sloped spectra. In Section VI a frequency-coherence model is developed and simple formulas for the random delay jitter and pulse dispersion derived from it.

Finally, in Section VII a model for angle scatter is developed. In all cases the formulas fully accommodate propagation at arbitrary incidence angles relative to the magnetic field. In deriving several of the formulas that might ultimately be used in a predictive code, we used a quadratic approximation, which is not strictly valid for the shallowly sloped spectra. Some refinements, therefore, may ultimately be desirable.

Wideband satellite data as well as data from the 1979 PLUMEX rocket campaign at Kwajalein are currently being analyzed and should show the degree to which the approximations are valid, at least in the natural

environment. In their present form, or with rather small modifications, the formulas summarized herein are adequate for current predictive modeling requirements.

II INTRODUCTION AND BACKGROUND

One objective of our channel modeling work has been to develop a mathematically tractable, but accurate characterization of the onset of phase and amplitude scintillation and the temporal, spatial, and frequency coherence of the disturbed radiowave. The coherence measures can be directly related to the scintillation-induced degradation of a variety of systems.

We have pursued a formal channel modeling approach, which takes advantage of the linearity of the transionospheric channel. If the complex signal, $v(t)$, is transmitted, for example, the received signal, $v_o(t)$, [less noise and interference] admits the representation

$$v_o(t) = \int \hat{v}(f) h(t;f+f_c) \exp\{2\pi i f t\}\, df \qquad (2.1)$$

where $\hat{v}(f)$ is the Fourier transform of $v(t)$, f_c is the center frequency, and $h(t;f)$ is the time-varying transfer function that characterizes the channel.

Formally, $h(t;f_c)$ is the response of the channel to a sinusoidal signal $\hat{v}(f) \sim \delta(f-f_c)$. The time structure comes about primarily because of the relative motion of the propagation path within the randomly irregular medium. In effect, the receiver sees a moving, spatially modulated, spherical wavefront. If $u(\vec{\rho},z;f_c)$ represents the spatial modulation, then

$$h(t,f_c) = u(\vec{v}_T t, v_z t; f_c) \qquad (2.2)$$

where $\vec{v} = (\vec{v}_T, v_z)$ is the instantaneous relative velocity. The scintillation problem, therefore, is mainly one of characterizing the spatial modulation imparted to a spherical wave by a random medium. The time structure is obtained by a straightforward translation.

There are two time and associated frequency intervals of interest in all communication systems: (1) a comparatively short time interval and its associated instantaneous bandwidth about f_c, which determines the basic modulation scheme (e.g., FSK, DPSK); and (2) a much longer time and frequency interval, over which coding and frequency hopping are employed. In almost all systems, $h(t;f+f_c)$ is nearly invariant over the sub-frequency band occupied by $\hat{v}(f)$. It them follows from Eq. (2.1) that

$$v_o(t) \cong h(t;f_c)v(t) \quad . \tag{2.3}$$

Scintillation is simply a complex (amplitude and phase) modulation imparted to the signal. Going further, if the time scale of $h(t;f_c)$ is long compared to the duration of $v(t)$, then $h(t;f_c)$ is effectively a complex constant. In such a "slow-fading" environment, only the amplitude variations affect the performance of a well-designed system.

As a practical matter, the Nakagami distribution

$$P(y) = \frac{m^m y^{m-1}}{\Gamma(m)} \exp\{-my\} \tag{2.4}$$

where y is the signal intensity, $m = S_4^{-2}$, S_4 is the intensity scintillation index, and

$$S_4^2 = (\langle I^2\rangle - \langle I\rangle^2)^{1/2}/\langle I\rangle \quad , \tag{2.5}$$

gives a very good approximation to the intensity statistics under all scatter conditions [see Fremouw et al. (1980)]. Moreover, under strong-scatter conditions, $S_4 \sim 1$ so that $m \sim 1$ and Eq. (2.4) takes the exponential form of the Rayleigh distribution.

We now know, however, that the complete Rayleigh model is not strictly applicable to signals undergoing strong scattering because of omnipresent, slow phase and associated amplitude variations. The impact of such subtle departures from strict Rayleigh scattering is discussed in

Rino (1979a,b). For predictive modeling, the departures from predictions based on the strict Rayleigh model are generally negligible.

The power of the Rayleigh model is that it is completely specified by the mutual coherence function

$$R_u(\delta t) = \langle h(t;f_c)h^*(t';f_c)\rangle \quad , \tag{2.6}$$

which is easily computed. In fact, for many applications one need only specify the coherence time, τ_c, such that

$$R_u(\tau_c) = K\, R_u(0) \tag{2.7}$$

where $K = e^{-1}$ or some other convenient fraction. In all our applications $R_u(0) = \langle I\rangle = 1$, that is the signal is normalized to unit intensity. A second useful relationship for Rayleigh channels is

$$\langle I(t)I(t')\rangle - 1 = |R_u(\delta t)|^2 \quad . \tag{2.8}$$

It follows from Eq. (2.8) that the intensity coherence time, τ_I, and the coherence time of the complex signal, τ_c, are simply related.

The first step in predictive modeling, therefore, is to determine the onset of saturated scintillation ($S_4 \sim 1$), where the Rayleigh model can be applied. The system effects under weak scintillation are easily determined from Eq. (2.4) and a rough estimate of the fade coherence time. To estimate the onset of saturated scintillation, we linearly extrapolate the weak scatter theory beyond its strict range of validity. This is a very conservative estimate because strong scatter effects always act to reduce the weak-scatter S_4 value. A detailed treatment of strong-scatter effects is presented in Rino (1979b, 1980). The weak-scatter theory is developed in Rino (1979a), but for convenience the principal formulas are summarized in Section III.

All our theoretical developments are based on the phase-screen model not only because of its simplicity, but because recent analyses show that results based on the phase-screen model preserve all essential aspects of much more elaborate calculations that properly accommodate the effects of diffraction within the scattering medium [Bramley (1977); Fante (1976)]. Furthermore, results based on the phase-screen model can, in many cases, be applied incrementally to accommodate variation along the propagation path (Rino, 1978).

In all our previous analysis, we have treated only the scattering of an incident plane wave. The plane-wave results, however, are easily generalized to accommodate the incident spherical wavefronts that eminate from a source at a finite distance. This is demonstrated in Section IV where the phase-screen model is applied to calculate the mutual coherence function.

The multiple-scatter theory, based on solutions to the parabolic wave equation, depends only on the integrated-phase structure function, as does the phase-screen theory. Because of its central role in the propagation theory, the form of the phase structure function in a general power-law environment and various approximations to it were discussed in detail in Topical Report 4. In Section V of this report we use those results to compute the mutual coherence function Eq. (2.6).

Precision navigation systems use very large bandwidths, and questions of frequency coherence become important. Thus, we have also computed the appropriate frequency-coherence function and used it to estimate the average delay jitter and coherence-bandwidth loss. The calculations are summarized in Section VI. To complete the channel model, in Section VII we compute the angular spectrum and derive formulas that characterize the angle scintillation. These formulas can be used for radar applications as well as relating the model calculations to previously developed radar codes.

In all cases, the model calculations reflect the critical dependence of the scintillation structure on the power-law index. If the index of the one-dimensional phase spectral density function is less than 3, the

statistical theory can be formulated completely without specifying the outer scale. As the spectrum steepens so that the phase spectral index exceeds 3, however, the outer scale must be specified to compute the mutual coherence function. In our model development we have generated formulas that apply to both the shallowly sloped and steeply sloped spectra.

III THE WEAK-SCATTER THEORY

For modeling purposes, we can ignore the inner scale cutoff. This has no effect on the phase variance, and at worst it over estimates the intensity scintillation at the highest frequencies of interest. The three-dimensional SDF that characterizes the striations has the form

$$\Phi_{\Delta N_e}(q) = \frac{abC_s}{[q_o^2 + q^2]^{\nu+1/2}} \tag{3.1}$$

where q_o is the outer-scale wave number, and a and b are the axial ratios along and transverse to the magnetic field respectively. The more general form of Eq. (3.1) that includes an inner-scale cutoff is discussed in Topical Report 4.

The isotropic turbulent strength C_s is related to the rms electron density $\langle \Delta N_e^2 \rangle$ by the relation

$$C_s = 8\pi^{3/2} \langle \Delta N_e^2 \rangle \, q_o^{2\nu-2} \, \Gamma(\nu+1/2)/\Gamma(\nu-1) \quad . \tag{3.2}$$

Since $\langle \Delta N_e^2 \rangle$ and q_o or the outer scale $\ell_o = 2\pi/q_o$ are most often specified, Eq. (3.2) can be used to calculate C_s. The autocorrelation function of the integrated phase has the form

$$R_{\delta\phi}(y) = r_e^2 \lambda^2 \ell_p G \, C_s \left| \frac{y}{2q_o} \right|^{\nu-1/2} \frac{K_{\nu-1/2}(q_o y)}{2\pi\Gamma(\nu+1/2)} \tag{3.3}$$

where r_e is the classical electron radius, λ is the wavelength, ℓ_p is the length of the propagation path, and $K_\nu(x)$ is the modified Bessel function.

To account fully for the spatial variation of the integrated phase, y in Eq. (3.3) must be replaced by

$$f(\vec{\Delta\rho}_s) = \left[\frac{C\Delta\rho_{s_x}^2 - B\Delta\rho_{s_x}\Delta\rho_{s_y} + A\Delta\rho_{s_y}^2}{AC - B^2/4}\right]^{1/2} \tag{3.4}$$

where

$$\vec{\Delta\rho}_s = \vec{\Delta\rho}_T - \tan\theta\ \hat{a}_{k_T}\Delta z \quad . \tag{3.5}$$

The angle, θ, is the angle of the propagation vector relative to the z axis and $\hat{a}_{k_T}$ is a unit vector along the projection of the propagation vector onto the plane normal to z. The reason Eq. (3.5) takes this particular form will become clear in Section IV.

The coefficients A, B, and C depend on the relative propagation angles and the anisotropy model. The geometrical enhancement factor, G, is defined in terms of A, B, and C as

$$G = \frac{ab}{\sqrt{AC - B^2/4}} \quad . \tag{3.6}$$

The anisotropy model is summarized in the Appendix.

The temporal phase autocorrelation function is obtained by substituting $\vec{v}_T\delta t$ and $v_z\delta t$ for $\vec{\Delta\rho}_T$ and Δz respectively in Eq. (3.5). The final form can be written compactly as $R_{\delta\phi}(v_{eff}\delta t)$, where

$$v_{eff} = \left[\frac{Cv_{s_x}^2 - Bv_{s_x}v_{s_y} + Av_{s_y}^2}{AC - B^2/4}\right]^{1/2} \tag{3.8}$$

and

$$\vec{v}_s = \vec{v}_T - \tan\theta\ \hat{a}_{k_T}v_z \quad . \tag{3.8}$$

The velocity vector $\vec{v} = (\vec{v}_T, v_z)$ is formally the relative velocity of the irregularities as seen by an observer in the reference coordinate system.

The one-dimensional phase SDF is obtained by taking the Fourier transform $R_{\delta\phi}(v_{eff}\delta t)$. The result is

$$\varphi(f) = \frac{T}{[f_o^2 + f^2]^{p/2}} \tag{3.9}$$

where

$$f_o = v_{eff}\, q_o/2\pi = v_{eff}\, \ell_o \quad , \tag{3.10}$$

and

$$T = r_e^2\lambda^2\, \ell_p G\, C_s \frac{\sqrt{\pi}\,\Gamma(\nu)}{(2\pi)^{2\nu+1}\Gamma(\nu+1/2)}\, v_{eff}^{2\nu-1} \tag{3.11}$$

In Eq. (3.9), $p = 2\nu$.

The phase variance can be computed by integrating Eq. (3.9) over all temporal frequencies, f. The result is

$$\langle\delta\phi^2\rangle = r_e^2\lambda^2\, \ell_p G\, C_s \frac{q_o^{-2\nu+1}\,\Gamma(\nu-1/2)}{4\pi\,\Gamma(\nu+1/2)} \quad . \tag{3.12}$$

In most cases, however, the length of the data interval, τ_c, is less than f_o^{-1} so that

$$\begin{aligned}\langle\delta\phi^2\rangle &\cong 2T\int_{\tau_c^{-1}}^{\infty} f^{-p}\, df \\ &= \frac{2T}{p-1}\,\tau_c^{p-1}\end{aligned} \tag{3.13}$$

To estimate the measured rms phase, one should use the minimum value of Eq. (3.12) or Eq. (3.13).

The corresponding intensity scintillation is given by the formula

$$S_4^2 = r_e^2 \lambda^2 \, \ell_p C_s Z^{\nu-1/2} \left[\frac{\Gamma\left(\frac{2.5-\nu}{2}\right)}{2\sqrt{\pi}\,\Gamma\left(\frac{\nu+0.5}{2}\right)(\nu-0.5)} \right] \mathcal{J} \tag{3.14}$$

where

$$\mathcal{J} = \frac{ab}{\sqrt{A''}\,C''^{\nu}} \, {}_2F_1\left(1/2 - \nu,\ 1/2,\ 1,\ \frac{A'' - C''}{A''}\right) \tag{3.15}$$

and

$$A'' = \frac{1}{2}[A' + C' + D'] \quad , \tag{3.16a}$$

$$C'' = \frac{1}{2}[A' + C' - D'] \tag{3.16b}$$

where

$$D' = \sqrt{(A' - C')^2 + B'^2} \quad . \tag{3.16c}$$

The parameter Z is the Fresnel parameter

$$Z = \frac{\lambda}{4\pi} \frac{R_1 R_2}{R_1 + R_2} \tag{3.17}$$

where R_1 is the signal-source-to-phase-screen distance and R_2 is the phase-screen-to-receiver distance. A simple series expansion can be used to evaluate the hypergeometric function. For actual computations we take the minimum value of Eq. (3.14) or unity. A predicted value of unity from Eq. (3.14) is a conservative estimate of where saturation actually occurs.

Equation (3.14) is strictly valid only when $\sqrt{Z} q_o \ll 1$, which is a good approximation at or above VHF for most propagation conditions. If $\sqrt{Z} q_o \gg 1$, however, it is easily shown that $S_4^2 \sim 2\sigma_\phi^2$. If $\sqrt{Z} q_o > 1$, the limiting value of $2\sigma_\phi^2$ can be used in place of the value given by Eq. (3.4) as a simple means of accommodating far-zone scattering. In an extended medium ℓ_p can be treated as a differential distance and

Eq. (3.12) or Eq. (3.13) and Eq. (3.14) integrated along the propagation path to accommodate the varying structure and propagation geometry.

Once the signal has saturated, one can use the Rayleigh model to predict the signal structure. As discussed in Section II, however, the strict applicability of the Rayleigh model is open to question. The power of the model is that it is completely specified by the mutual coherence function. We also note in passing that under weak-scatter conditions the intensity coherence time τ_I generally satisfies the inequality,

$$\tau_I < \sqrt{Z}/v_{eff} \quad . \tag{3.18}$$

This is discussed in detail by Rino and Owen (1980).

IV THE PHASE-SCREEN MODEL

The phase-screen model proceeds formally from the Huygens-Fresnel principle, which for our purposes can be written as

$$u(\vec{r}) = C_H \iint u(\vec{r}\,')G(\vec{r},\vec{r}\,')\, d\vec{r}\,' \tag{4.1}$$

where

$$G(\vec{r},\vec{r}\,') = \frac{\exp\{-ik|\vec{r} - \vec{r}\,'|\}}{|\vec{r} - \vec{r}\,'|} \tag{4.2}$$

and the complex constant C_H will be determined later [see Born and Wolf (1964), Chapter 8 for a detailed discussion]. If $u(\vec{\rho},z_o)$ is known, we can write

$$u(\vec{\rho},z) = C_H \iint u(\vec{\kappa};z_o) \iint G(\vec{r},\vec{r}\,') \exp\{-i\vec{\kappa} \cdot (\vec{\rho} - \vec{\rho}\,')\}\, d\vec{\rho}\,'$$

$$\times \exp\{-i\vec{\kappa} \cdot \vec{\rho}\} \frac{d\vec{\kappa}}{(2\pi)^2} \tag{4.3}$$

where $u(\vec{\kappa};z_o)$ is the Fourier spectrum of $u(\vec{\rho},z_o)$. For notational convenience we let $z_o = 0$ when its value enters explicitly.

The inner integral can be evaluated [see Rino and Fremouw (1977), Eq. (5)]. Substituting that result into Eq. (4.3) and changing variables from $\vec{\kappa}$ to $\vec{\kappa} + \vec{k}_T$ gives

$$u(\vec{\rho},z) = -i\lambda C_H \iint \hat{u}(\vec{\kappa} + \vec{k}_T) \frac{\exp\{-ikg(\vec{\kappa} + \vec{k}_T)z\}}{g(\vec{\kappa} + \vec{k}_T)} \exp\{-i\vec{\kappa} \cdot \vec{\rho}\} \frac{d\vec{\kappa}}{(2\pi)^2}$$

$$\times \exp\{-i\vec{k}_T \cdot \vec{\rho}\} \tag{4.4}$$

where

$$g(\vec{\kappa} + \vec{k}_T) = k\left[1 - \frac{(\vec{\kappa} + \vec{k}_T)^2}{k}\right]^{1/2} \tag{4.5}$$

To approximate Eq. (4.5) we first define cos θ as

$$\cos\theta = \frac{\vec{k} \cdot \hat{a}_z}{k} \tag{4.6}$$

so that

$$g(\vec{\kappa} + \vec{k}_T) = \cos\theta\left[1 - \left(\frac{\kappa}{k\cos\theta}\right)^2 - \frac{2\tan\theta\,\vec{\kappa}\cdot\hat{a}_{k_T}}{k\cos\theta}\right]^{1/2} \tag{4.7}$$

Under conditions of narrow-angle scattering, it is permissible to retain only the second-order terms in the Taylor series expansion of Eq. (4.7) in the exponential term in Eq. (4.4) and only the leading term in the denominator. The result is

$$u(\vec{\rho},z) = \iint u(\vec{\kappa} + \vec{k}_T)\,\exp\left\{-ih(\vec{\kappa})\,\frac{z\sec\theta}{2k}\right\} \times \exp\{-i\vec{\kappa}\cdot\vec{\rho}_s\}\,\frac{d\vec{\kappa}}{(2\pi)^2}\,\exp\{-k\cos\theta\,z\} \tag{4.8}$$

where

$$h(\vec{\kappa}) = \kappa^2 + \left(\hat{a}_{k_T}\cdot\vec{\kappa}\tan\theta\right)^2 \tag{4.9}$$

and

$$\vec{\rho}_s = \vec{\rho} + \tan\theta\,\hat{a}_{k_T} z \quad . \tag{4.10}$$

We have set C = i sec θ/λ so that Eq. (4.8) is a proper solution to the parabolic wave equation.

Now consider an incident spherical wave

$$u_i = \frac{\exp\left\{-ik\left|\vec{R}_1 + \vec{\rho}\right|\right\}}{\left|\vec{R}_1 + \vec{\rho}\right|} \tag{4.11}$$

where $\vec{R}_1$ is the distance from the point source to the plane $z = z_o$ and $\vec{\rho}$ lies within the plane. If $R_1 \gg \rho$, we can write

$$u_i \sim \frac{\exp\left\{-ikR_1\right\}}{R_1} \exp\left\{-i\left(\vec{k}_T \cdot \vec{\rho} + \frac{k}{2}\frac{\rho^2 - \sin^2\theta\left(\hat{a}_{k_T} \cdot \vec{\rho}\right)^2}{R_1}\right)\right\} . \tag{4.12}$$

Replacing the reference wave, $\exp\{ikR_1\}/R_1$, by a more general modulation, $u(\vec{\rho},z_o)$, we have

$$u(\vec{\kappa} + \vec{k}) = \iint u(\vec{\rho}',z_o) \exp\left\{-\frac{k}{2}\frac{\rho'^2 - \sin^2\theta\left(\hat{a}_{k_T} \cdot \vec{\rho}'\right)^2}{R_1}\right\} \exp\{-i\vec{\kappa} \cdot \vec{\rho}'\}\, d\vec{\rho}' . \tag{4.13}$$

Substituting Eq. (4.13) into Eq. (4.8) gives

$$u(\vec{\rho},z) = \iint u(\vec{\rho}',z_o) \exp\left\{-\frac{k}{2}\frac{\rho'^2 - \sin^2\theta\left(\hat{a}_{k_T} \cdot \rho'\right)^2}{R_1}\right\} \times \iint \exp\left\{-ih(\vec{\kappa})\frac{z \sec\theta}{2k}\right\} \exp\{i\vec{\kappa} \cdot (\vec{\rho}' - \vec{\rho}_s)\} \frac{d\vec{\kappa}}{(2\pi)^2}\, d\vec{\rho}' \tag{4.14}$$

The integral over $\vec{\kappa}$ can be evaluated as

$$I = -i\frac{\cos\theta}{4\pi z} \exp\left\{-i\frac{k}{2}\frac{\eta^2 - \sin^2\theta\left(\hat{a}_{k_T} \cdot \vec{\eta}\right)^2}{z \sec\theta}\right\} \tag{4.15}$$

where $\vec{\eta} = \vec{\rho} - \vec{\rho}_s$ and R_2 is the propagation distance from $z = z_o$ ($R_2 = z \sec\theta$). Thus

$$u(\vec{\rho},z) = \frac{k \cos\theta}{2\pi i R_2} \iint u(\vec{\rho},z_o) \exp\left\{-i \frac{k}{2R_e}\left[(\vec{\rho}' - C\vec{\rho}_s)^2 - \sin^2\theta\left(\hat{a}_{k_T} \vec{\rho}' - C\vec{\rho}_s\right)^2\right]\right\} d\vec{\rho}$$

$$\times \exp\left\{-i \frac{k}{(R_1 + R_2)}\left[\rho_s^2 - \sin^2\theta\left(\hat{a}_{k_T} \cdot \vec{\rho}_s\right)^2\right]\right\} \tag{4.16}$$

where

$$R_e = \frac{R_1 R_2}{R_1 + R_2} \tag{4.17}$$

and

$$C = \frac{R_1}{R_1 + R_2} \quad . \tag{4.18}$$

It follows from Eq. (4.16) that aside from a small phase modulation, the effects of a point source of illumination can be accommodated simply by replacing $\vec{\rho}_s$ by $C\vec{\rho}_s$ and the propagation distance (z sec θ) by $R_1R_2/(R_1+R_2)$. Thus, any result based on plane waves is readily modified to accommodate spherical waves.

Equation (4.16) also shows the effects of an interchange of source and receiver (R_1 and R_2). Insofar as effects that depend on propagation distance are concerned, reciprocity holds. Structure variations, however, depend on C, and they do change. As a practical matter, only S_4 and other single-point measurements, such as the frequency-coherence measures described in Section VI are reciprocal. Spatial and temporal coherence measures (second-order moments) are not reciprocal.

Equation (4.16) or its Fourier domain equivalent form the starting point for all phase-screen computations. Hereafter, however, we shall apply the plane wave form and simply insert the spherical wave correction factors where appropriate. This has already been done in Eq. (3.17)

V THE MUTUAL COHERENCE FUNCTION

As discussed in Section II, under conditions of Rayleigh scattering the mutual coherence function completely specifies the average signal structure. To compute $\langle u(\vec{\rho},z)u^*(\vec{\rho};z')\rangle$, we use the Huygens-Fresnel formula Eq. (4.8) together with the homogeneity assumption

$$\langle u(\vec{\kappa})u^*(\vec{\kappa}')\rangle = \Phi_u(\vec{\kappa})\delta(\vec{\kappa} - \vec{\kappa}') \tag{5.1}$$

as discussed by Rino and Fremouw (1977). In Eq. (5.1), $\Phi_u(\vec{\kappa})$ is the SDF of $u(\vec{\rho},z_o)$ and $\delta(\vec{\kappa})$ denotes the Kronecker delta function. The result is

$$\langle u(\vec{\rho},z)u^*(\vec{\rho}'z')\rangle = \iint \Phi_u(\vec{\kappa} + \vec{k}_T)\ \exp\left\{-ih(\vec{\kappa})\ \frac{\Delta z\ \sec\ \theta}{2k}\right\} \times \exp\left\{-i\vec{\kappa}\cdot\Delta\vec{\rho}_s\right\}\ \frac{d\vec{\kappa}}{(2\pi)^2} \tag{5.2}$$

where $\Delta z = z - z'$, $\Delta\vec{\rho} = \vec{\rho} - \vec{\rho}'$, and $\Delta\vec{\rho}_s = \Delta\vec{\rho} - \tan\theta\ \hat{a}_{k_T}\Delta z$.

It is simpler to specify the mutual coherence function than the angular spectral density $\Phi_u(\vec{\kappa} + \vec{k}_T)$. We note, however, that if $\Delta z = 0$, Eq. (5.2) shows that

$$\langle u(\vec{\rho},z)u^*(\vec{\rho}',z)\rangle = R_u(\Delta\vec{\rho}_s) \quad . \tag{5.3}$$

Indeed, for most applications the Δz dependence can be ignored. Nonetheless, by using Eq. (4.15) it is readily shown that

$$R_u(\Delta\vec{\rho},\Delta z) = \iint R_u(\Delta\vec{\rho}' + \Delta\vec{\rho}_s)\ \frac{k\ \cos\ \theta}{2\pi i\Delta R_2} \times\ \exp\left\{-i\ \frac{k}{2\Delta R_2}\left[\Delta\rho'^2 - \sin^2\theta\left(\hat{a}_{k_T}\cdot\Delta\vec{\rho}'\right)^2\right]\right\} d\Delta\vec{\rho}' \quad , \tag{5.4}$$

where we have substituted ΔR_2 for Δz sec θ.

In the phase-screen model,

$$R_u(\vec{\Delta\rho}) = \exp\left\{-\frac{1}{2}D_{\delta\phi}(\vec{\Delta\rho}_s)\right\} \tag{5.5}$$

where $D_{\delta\phi}(\vec{\Delta\rho})$ is the integrated-phase structure function. Two approximate forms for $D_{\delta\phi}(y)$ have been developed. If the ν parameter [see Eq. (3.1)] is less than 1.5,

$$D_{\delta\phi}(y) \sim C_{\delta\phi}^2 |y|^{2\nu-1} \tag{5.6}$$

where $C_{\delta\phi}^2$ is the phase-structure constant

$$C_{\delta\phi}^2 = G\frac{C_p}{2\pi}\frac{2\Gamma(1.5-\nu)}{\Gamma(\nu+0.5)(2\nu-1)^{2\nu-1}} \quad . \tag{5.7}$$

In Eq. (5.7), $C_p = r_e^2\lambda^2\ell_p C_s$. A detailed derivation of Eq. (5.6) and a demonstration of its range of validity can be found in Topical Report 4.

If $\nu \geq 1.5$, the situation is more complicated. The overall convergence of the Taylor series is too slow for it to be of general practical applicability. It happens, however, that the quadratic term alone does an acceptable job of reproducing the exact form of $D_{\delta\phi}(y)$ for $q_o|y| \ll 1$ when $\nu > 1.5$. Thus, we take

$$D_{\delta\phi}(y) \sim 2\sigma_\phi^2 D_1 (q_o y)^2 \tag{5.8}$$

where

$$D_1 \sim \begin{cases} \frac{1}{2}\log(2\epsilon) & \nu = 1.5 \quad , \\ \frac{\Gamma(\nu-1.5)}{4\Gamma(\nu-0.5)} & \nu > 1.5 \quad , \end{cases} \tag{5.9}$$

and $\epsilon \ll 1$ is the ratio of the outer- to inner-scale wave numbers. Note that Eq. (5.8) depends on q_o and, when $\nu = 1.5$, the inner scale as well. Again, a detailed discussion is given in Topical Report 4.

In general, therefore,

$$D_{\delta\phi}(y) \sim D_\nu |y|^{\min(2\nu-1,2)} \tag{5.10}$$

where D is replaced by Eq. (5.7) when $\nu < 1.5$ and $2\sigma_\phi^2 D_1 q_o^2$ with D_1 given by Eq. (5.9) when $\nu \geq 1.5$. Unfortunately, Eq. (5.4) cannot be evaluated analytically when $\nu < 1.5$. If $\nu \geq 1.5$, however, it can be shown that

$$R_u(\vec{\Delta\rho},\Delta R_2) = \frac{R_u(\vec{\Delta\rho}_s)}{\sqrt{\left(1 - i\frac{D_\nu \Delta R_2}{k\cos^2\theta}\right)\left(1 - i\frac{D_\nu \Delta R_2}{k}\right)}} \times \exp\left\{-i\frac{D_\nu^2 \Delta R_2}{2k}\left[\frac{\Delta\rho_s^2}{\left(1 - i\frac{D_\nu \Delta R_2}{k}\right)} + \frac{\tan^2\theta\left(\hat{a}_{k_T}\cdot\Delta\rho_s\right)^2}{\left(1 - i\frac{D_\nu \Delta R_2}{k}\right)\left(1 - \frac{D_\nu \Delta R_2}{k\cos^2\theta}\right)}\right]\right\} \tag{5.11}$$

If $|\vec{\Delta\rho}| \gg \Delta R_2$ as is usually the case, then

$$R_u(\vec{\Delta\rho},\Delta R_2) \sim \exp\left\{-\frac{1}{2} D_\nu |\vec{\Delta\rho}_s|^{\min(2\nu-1,2)}\right\} \quad . \tag{5.12}$$

If $\Delta R_2 \gg |\vec{\Delta\rho}|$, however,

$$|R_u(\vec{\Delta\rho},\Delta R_2)| \sim \frac{1}{\left(1 + \frac{D_\nu \Delta R_2}{k}\right)^2} \tag{5.13}$$

provided that θ is not too large.

To characterize the measured signal when Eq. (5.12) applies, we have

$$R_u(\delta t) = \exp\left\{-\frac{1}{2} D_\nu |Cv_{eff}\delta t|^{\min(2\nu-1,2)}\right\} \quad . \tag{5.14}$$

The C factor as defined by Eq. (4.18) corrects for wavefront curvature. If Eq. (5.3) applies, we have, similarly,

$$|R_u(\delta t)| \sim \frac{1}{\left(1 + \frac{D_\nu v_\parallel}{k}\,\delta t\right)^2} \tag{5.15}$$

where $v_\parallel$ is the rate of change of R_e as defined by Eq. (4.17). From Eqs. (5.14) and (2.7) with $K = e^{-1}$ it follows that

$$\tau_c = \frac{1}{v_{eff} C}\left[\frac{2}{D_\nu}\right]^{\frac{1}{\min(2\nu-1,2)}} . \tag{5.16}$$

Under Rayleigh scatter conditions, moreover, it follows from Eq. (2.8) that

$$\tau_I = \frac{1}{v_{eff} C}\left[\frac{1}{D_\nu}\right]^{\frac{1}{\min(2\nu-1,2)}} . \tag{5.17}$$

Similar definitions for $\tau_\parallel$ can be deduced from Eq. (5.15). As a practical matter, $\tau_\parallel$ can be applied as an upper bound on τ_c when v_{eff} is small as suggested by L. Wittwer. To accommodate properly geometric and source variations in an extended medium, the argument of the exponential in Eq. (5.12) must be integrated along the propagation path. The integrated equations can then be inverted to evaluate τ_c or τ_I.

VI COHERENCE BANDWIDTH

Loss of coherence bandwidth causes group-delay jitter and pulse dispersion. Such effects are potentially disruptive to spread spectrum systems such as the Global Positioning System (GPS). The dispersive effects can be characterized by the temporal moments

$$M_n = \int_{-\infty}^{\infty} t^n \langle |v_o(t)|^2 \rangle \, dt \quad . \tag{6.1}$$

Yeh and Liu (1977) have shown, for example, that

$$\tau_d \triangleq M_1 = \frac{1}{2\pi i} \int_{-F/2}^{F/2} |\hat{v}(f)|^2 \left[\frac{\partial}{\partial \delta f} R(\delta f;\, f + f_c) \right]_{\delta f = 0} df \tag{6.2}$$

and

$$\Omega_d \triangleq M_2 - \int t^2 \, |v(t)|^2 \, dt$$

$$= \frac{1}{2\pi i} \int_{-F/2}^{F/2} |v(f)|^2 \left[\frac{\partial^2}{\partial \delta f^2} R(\delta f;\, f + f_c) \right]_{\delta f = 0} df \tag{6.3}$$

where F is the bandwidth, f_c is the center frequency, and

$$R(\delta f; f) = \langle u(t, f + \delta f/2) u^*(t; f - \delta f/2) \rangle \tag{6.4}$$

is the single-point, two-frequency coherence function.

To calculate $R(\delta f; f)$ we use the Huygens-Fresnel formula Eq. (4.16). Because Eq. (6.4) applies only to a single point, however, it is unnecessary to preserve the full generality of Eq. (4.16). We, therefore, need only consider

$$u(\vec{\rho}_\perp, R_e; f_1) = \frac{1}{2\pi i R_e} \iint \exp\left\{-i\xi^2 \frac{k_1}{2z_\ell}\right\} u(\vec{\rho}_\perp + \vec{\xi}, 0; f_1)\, d\vec{\xi} \tag{6.5}$$

from which

$$R(\delta f; f) = \frac{1}{2\pi i} \frac{k_1 k_2}{(k_1 - k_2)R_e} \iint \exp\left\{i \frac{\Delta\xi^2}{2} \frac{k_1 k_2}{(k_1 - k_2)z_\ell}\right\} R_u(\Delta\vec{\xi};\, f_1, f_2)\, d\Delta\vec{\xi} \tag{6.6}$$

follows after a variable change and some straightforward manipulations. In Eq. (6.6) k_1 and k_2 are the wave numbers corresponding to $f_1 = f - \delta f/2$ and $f_2 = f + \delta f/2$ respectively and $\vec{\rho}_\perp$ is measured transverse to the line of sight.

To calculate $R_u(\Delta\vec{\xi}; f_1, f_2)$, we use the phase-screen model. If $\epsilon = \delta f/(2f)$ is small, it can be shown that

$$R_u(\Delta\vec{\xi}; \delta f; f) = \exp\left\{-D_{\delta\phi}(\Delta\vec{\xi})\right\} \exp\left\{-2\epsilon^2 \sigma_\phi^2\right\} \tag{6.7}$$

where σ_ϕ^2 and $D(\Delta\vec{\xi})$ are evaluated at the mean frequency, f. (Note that f need not equal f_c).

By making a consistent approximation of $(k_1 k_2)/(k_1 - k_2)$, changing variables in Eq. (6.6), and substituting into Eq. (6.7), we obtain the general result

$$R(\delta f; f) = \frac{i}{2\pi} \iint \exp\left\{-i\,\Delta\xi^2/2\right\} \exp\left\{-D_{\delta\phi}(\Delta\vec{\xi}[2Z\,\delta f/f]^{1/2})\right\} d\Delta\xi \exp\left\{-\sigma_\phi^2\, 2\epsilon^2\right\} \tag{6.8}$$

Since we are working in a transverse coordinate system, $D_{\delta\phi}(\Delta\vec{\xi})$ is functionally dependent on the quadratic form

$$y^2 = \frac{C'\Delta\xi_x^2 - B'\Delta\xi_x\Delta\xi_y + A'\Delta\xi_y^2}{A'C' - B'^2/4} \tag{6.9}$$

where A', B', and C' are defined by Eqs. (26a, 26b, and 26c) by Rino (1979a). For convenience the definitions are summarized in the Appendix.

By first rotating variables to remove the $\Delta\xi_x\Delta\xi_y$ term and then performing a series of variable changes, Eq. (6.8) can be reduced to the single integral

$$R(\delta f;f) = i\sqrt{\beta^2-\alpha^2}\int_0^\infty J_0(\omega\alpha)\exp\{-i\omega\beta\} \times \exp\left\{-D_\phi\left([\omega 2Z\,\delta f/f]^{1/2}\right)\right\} d\omega \exp\{-\sigma_\phi^2\, 2\epsilon^2\} \tag{6.10}$$

where

$$A'' = \tfrac{1}{2}(A' + C' + D') \tag{6.11a}$$

$$C'' = \tfrac{1}{2}(A' + C' - D') \tag{6.11b}$$

$$D' = \sqrt{(A' - C')^2 + B'^2} \tag{6.11c}$$

$$\alpha = (A'' - C'')/4 \tag{6.11d}$$

$$\beta = (A'' + C'')/4 \tag{6.11e}$$

and Z is defined by Eq. (3.17). The same transformation was used to derive Eq. (3.14) [cf. Eqs. (3.16a), (3.16b), and (3.16c)]. For isotropic irregularities $A'' = C'' = 1$ so that $\beta = 0.5$ and $\alpha = 0$. For highly anisotropic irregularities, $A'' \sim a^2$ where a is the axial ratio, and $C'' = 1$. For large a, $\alpha \sim \beta$ although $\beta^2 - \alpha^2 \cong A''C''/4$.

If the small q_o approximation Eq. (5.6) is used,

$$D([\omega 2Z\delta f/f]^{1/2}) \sim C_{\delta\phi}^2\,[2Z\delta f/f]^{\nu-0.5}\omega^{\nu-0.5} \tag{6.12}$$

Unfortunately Eq. (6.10) cannot be evaluated analytically for arbitrary ν values within the admissible range $5 < \nu < 1.5$. However, if ν in Eq. (6.12) is set equal to 1.5 without changing the definition of $C_{\delta\phi}^2$, then Eq. (6.10) can be evaluated giving the result,

$$R(\delta f;f) \cong \frac{\sqrt{\beta^2 - \alpha^2}\ \exp\{-\sigma_{\delta\phi}^2\ 2\epsilon^2\}}{\sqrt{(\beta - iH|\delta f/f|)^2 - \alpha^2}} \tag{6.13}$$

where

$$H = C_{\delta\phi}^2\ 2Z \tag{6.14}$$

Alternatively, we can use the quadratic approximation Eq. (5.8), whereby

$$D\left([\omega 2Z\delta f/f]^{1/2}\right) \cong \left(2\sigma_\phi^2\ D_1 q_o^2\right) 2Z|\delta f/f| \tag{6.15}$$

This gives rise to a form identical to Eq. (6.13), but with H replaced by

$$H_q = 2\sigma_{\delta\phi}^2\ D_1 q_o^2 \tag{6.16}$$

The form Eq. (6.13) can be regarded as exact for the more steeply sloped SDFs where the quadratic approximation can be applied.

If Eq. (6.13) is used in Eqs. (6.2) and (6.3), assuming that $|\delta f/f| \ll 1$, then

$$\tau \cong \left(\frac{H}{2\pi f_c}\right)\left(\frac{\beta}{\beta^2 - \alpha^2}\right) \tag{6.17}$$

and

$$\Omega_d \cong \left(\frac{H}{2\pi f_c}\right)^2 \frac{\beta^2 + \alpha^2}{(\beta^2 - \alpha^2)^2} \tag{6.18}$$

For highly anisotropic irregularities $\beta/(\beta^2 - \alpha^2) \sim 1$ and $\Omega_d = 2\tau_d^2$. Equations (6.17) and (6.18) are simplified forms of similar expressions derived by Fante (1978) and Yeh and Liu (1977). The simplifications arise mainly because the phase-screen model was used.

To give some idea of the order of magnitude of the expected delay jitter, in Figure 1, τ_d is plotted against C_s. The parameter values listed on the figure are the same as were used for the equatorial S_4 calculations presented by Rino (1979a). The quadratic approximation is also plotted for $\ell_o = q_o/2\pi = 10$ km. The results show that under conditions that produce strong gigahertz scintillation, 1 ns to 3 ns of delay jitter can occur, which is in agreement with the calculations of Yeh and Liu (1977).

The results have not yet been tested against real data. Analysis of the Wideband satellite data is currently being pursued; moreover, a GPS receiver system will be operated at the equator in the summer of 1980, in part to evaluate the receiver performance under disturbed conditions. For the present, the model formulas are adequate for system performance evaluation. It should be noted that only the random component of the group delay is included in Eqs. (6.17) and (6.18). The steady component must be added. The smooth dispersive delay constitutes a bias that must be accommodated in using the GPS system.

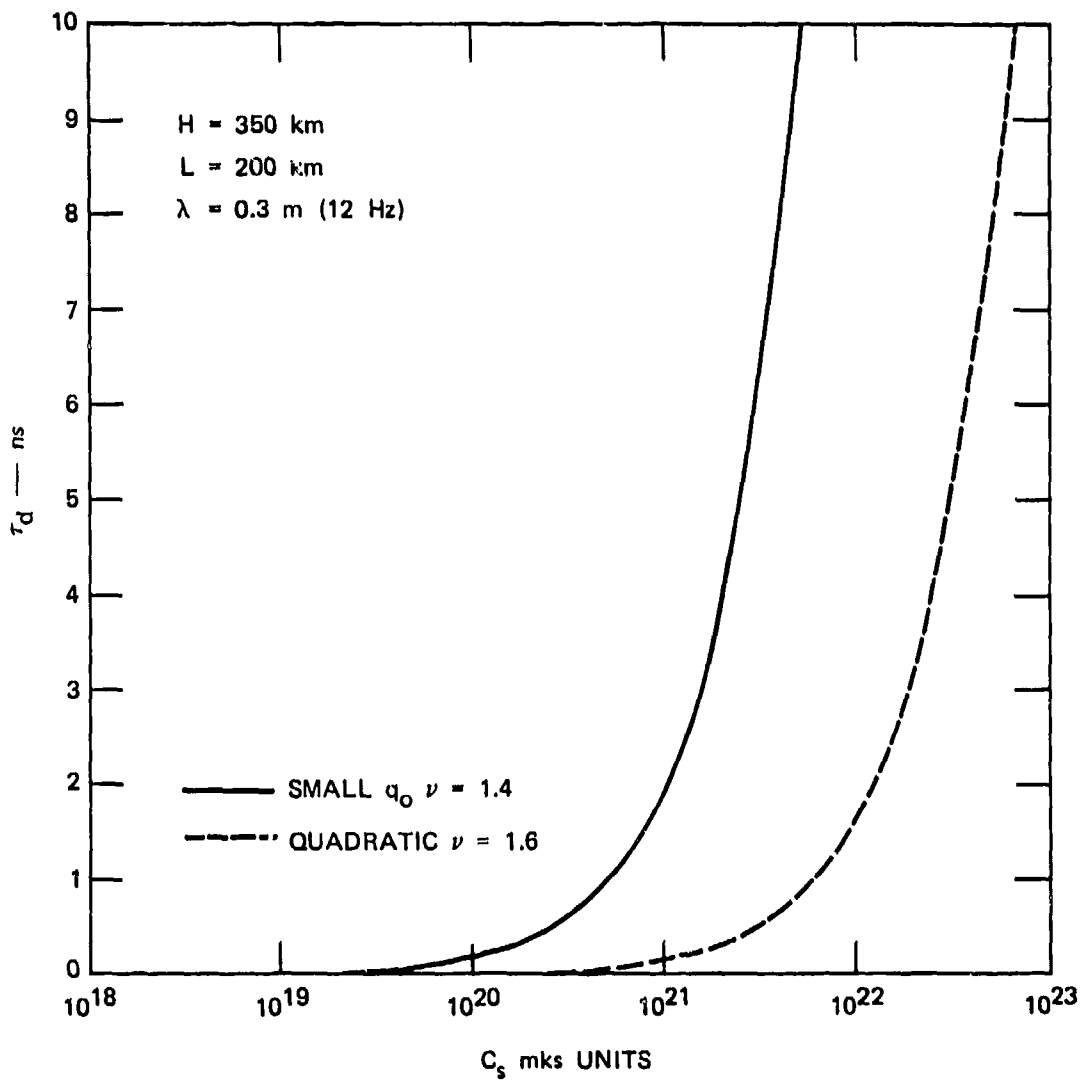

FIGURE 1 THEORETICAL CALCULATIONS OF DELAY JITTER CAUSED BY LOSS OF COHERENCE BANDWIDTH

VII ANGULAR SCATTERING

To analyze radar system performance, we need a direct measure of the angular fluctuations of the incident wavefront. As we have computed it, the mutual coherence function Eq. (5.5) gives the three-dimensional spatial correlation of the wavefield. To compute the angular spectrum, therefore, we must compute the two-dimensional Fourier transform of $R_u(\Delta\vec{\rho},\Delta z)$ in a plane perpendicular to $\vec{k}$.

In the plane normal to $\vec{k}$, the mutual coherence function has the form

$$R_u(\Delta\rho_\perp) = \exp\left\{-\frac{1}{2}D_{\delta\phi}(y_\perp)\right\} \tag{7.1}$$

where

$$y_\perp = \left[\frac{C'\Delta\rho_{\perp x}^2 - B'\Delta\rho_{\perp x}\Delta\rho_{\perp y} + A'\Delta\rho_{\perp y}^2}{A'C' - B'^2/4}\right]^{1/2} . \tag{7.2}$$

The x-axis here lies in the plane of $\bar{k}$ and the magnetic field vector. The form of the structure does not change aside from replacing A, B, and C in Eq. (3.4) by A′, B′, and C′. As was the case for the single-point two-frequency coherence function, however, the integral can only be evaluated analytically under the quadratic approximation.

Using Eq. (5.10), it follows from Eq. (7.1) that

$$\Phi_A(\kappa_{\perp x},\kappa_{\perp y}) = \frac{1}{2\pi D_\nu C^2}\exp\left\{-\frac{q_\perp^2}{2D_\nu C^2}\right\} \tag{7.3}$$

where

$$q_\perp^2 = \frac{A'\kappa_{\perp x}^2 + B'\kappa_{\perp x}\kappa_{\perp y} + C'\kappa_{\perp y}^2}{A'C' - B'^2/4} \tag{7.4}$$

and C is the spherical wavefront correction Eq. (4.18). To convert to scattering angles, we need only replace $K_{\perp x}$ and $K_{\perp y}$ by $k\delta\phi_x$ and $k\delta\phi_y$ respectively. $\delta\phi_x$ is the scattering angle in the plane of $\vec{k}$ and the magnetic field vector.

Note that $q_\perp^2$ = const. defines a quadratic form. The axial ratio is given by the formula

$$AR = [(A' + C' + D')/(A' + C' - D')]^{1/2} \tag{7.5}$$

where

$$D' = \sqrt{(A' - C')^2 + B'^2} \tag{7.6}$$

The maximum scattering occurs at an angle

$$\phi_R = \frac{1}{2} \operatorname{atan}\left[\frac{B'}{A' - C'}\right] \tag{7.7}$$

relative to the x axis.

The material in this section is a straightforward generalization of earlier work by Hardin and Tappert (1974). The results herein characterize the average angular scattering in a three-dimensional power-law medium, subject to the limitations imposed by the approximations used to derive a simple analytic form for the angular spectrum.

REFERENCES

Born, M. and E. Wolf, Principles of Optics, Ch. 8, (The MacMillan Company, New York, N.Y., 1964).

Bramley, E. M., "The Accuracy of Computing Ionospheric Radio-Wave Scintillation by the Thin-Phase-Screen Approximation," J. Atmos. Terr. Phys., Vol. 39, p. 367 (1977).

Briggs, B. H. and I. A. Parkin, "On the Variation of Radio Star and Satellite Scintillations with Zenith Angle," J. Atmos. Terr. Phys., Vol. 25, p. 339 (1963).

Fante, R. L., "Multiple-Frequency Mutual Coherence Functions for a Beam in a Random Medium," IEEE Trans. Ant. and Prop., Vol. AP-26, p. 621 (1978).

Fante, R. L., "Comparison of Theories for Intensity Fluctuations in Strong Turbulence," Radio Science, Vol. 11, p. 215 (1976).

Fremouw, E. J., R. C. Livingston, and D. A. Miller, "On the Statistics of Scintillating Signals," J. Atmos. Terr. Phys., submitted (1980).

Hardin, R. H. and F. D. Tappert, "Analysis, Simulation, and Models of Ionospheric Scintillation," Joint Radar Propagation Study, Contracts DAHC60-71-C-0005 and F19628-73-C-0002, Western Electric, Whippany, NJ (1974).

Knepp, D. L. and R. L. Bogusch, "Predictions of GPS X-Set Performance During the Places Experiment," DNA 5038T, Topical Report, Contract DNA001-78-C-0364, Mission Research Corp., Santa Barbara, CA (1978).

Rino, C. L., "Numerical Computations for a One-Dimensional Power-Law Phase Screen," Radio Science, in press (1980).

Rino, C. L., "A Power-Law Phase Screen Model for Ionospheric Scintillation 1. Weak Scatter," Radio Science, Vol. 14, p. 1135 (1979a).

Rino, C. L., "A Power-Law Phase Screen Model for Ionospheric Scintillation 2. Strong Scatter," Radio Science, Vol. 14, p. 1147 (1979b).

Rino, C. L., "Iterative Methods for Treating the Multiple Scattering of Radio Waves," J. Atmos. Terr. Phys., Vol. 40, p. 1011 (1978).

Rino, C. L. and E. J. Fremouw, "The Angle Dependence of Singly Scattered Wavefields," J. Atmos. Terr. Phys., Vol. 39, p. 859 (1977).

Rino, C. L. and J. Owen, "The Structure of Localized Nighttime Auroral-Zone Scintillation Enhancements," J. Geophys. Res., submitted (1980).

Rufenach, C. L., "Ionospheric Scintillation by a Random Phase Screen: Spectral Approach," Radio Science, Vol. 10, p. 155 (1975).

Singleton, D. G., "The Dependence of High-Latitude Ionospheric Scintillations on Zenith Angle and Azimuth," J. Atmos. Terr. Phys., Vol. 35, p. 2253 (1973).

Yeh, K. C. and C. H. Liu, "An Investigation of Temporal Moments of Stochastic Waves," Radio Science, Vol. 12, p. 671 (1977).

Appendix

ANISOTROPY COEFFICIENTS

In Rino and Fremouw (1977) it is shown that the two-dimensional phase SDF, $\Phi_{\delta\phi}(\vec{\kappa})$, is related to the three-dimensional irregularity SDF $\Phi_{\Delta N_e}(\vec{\kappa},\kappa_z)$ by the relation

$$\Phi_{\delta\phi}(\vec{\kappa}) = r_e^2\lambda^2 \, L \sec^2\theta \, \Phi_{\Delta N_e}\left(\vec{\kappa}, -\tan\theta \, \hat{a}_{k_T} \cdot \vec{\kappa}\right) \quad . \tag{1}$$

Now, if we assume that there exists a coordinate system (r, s, t) in which which the three-dimensional spatial correlation depends only on $[\Delta r^2 + (\Delta s/a)^2 + (\Delta r/r)^2]^{1/2}$, with a and b $\geq$ 1, the corresponding functional dependence of $\Phi_{\Delta N_e}(\vec{\kappa},\kappa_z)$ on $\vec{\kappa}$ and κ_z can be computed by straightforward manipulations.

The functional dependence is given in terms of the quadratic form $[(\vec{\kappa},\kappa_z)^T\hat{\underset{\sim}{C}}(\vec{\kappa},\kappa_z)]^{1/2}$ where $\hat{\underset{\sim}{C}}$ is a 3 x 3 matrix with elements:

$$\hat{C}_{11} = a^2\cos^2\psi + \sin^2\psi(b^2\sin^2\delta + \cos^2\delta) \tag{2a}$$

$$\hat{C}_{22} = b^2\cos^2\delta + \sin^2\delta \tag{2b}$$

$$\hat{C}_{33} = a^2\sin^2\psi + \cos^2(b^2\sin^2\delta + \cos^2\delta) \tag{2c}$$

$$\hat{C}_{12} = \hat{C}_{21} = (b^2 - 1)\sin\psi\sin\delta\cos\delta \tag{2d}$$

$$\hat{C}_{13} = \hat{C}_{31} = (a^2 - b^2\sin^2\delta - \cos^2\delta)\sin\psi\cos\psi \tag{2e}$$

$$\hat{C}_{23} = \hat{C}_{32} - (b^2 - 1)\cos\psi\sin\delta\cos\delta \quad . \tag{2f}$$

Note that if b = 1, then $\hat{C}_{12} = \hat{C}_{21} = \hat{C}_{23} = \hat{C}_{32} = 0$. The angle ψ is the dip angle. The angle δ is the orientation angle of the transverse irregularity axis. The angle, θ, is the zenith angle of $\vec{k}$ and φ is the magnetic azimuth.

The coefficients, A, B, and C, are readily deduced by substituting $-\tan\theta\ \hat{a}_{k_T} \cdot \vec{K}$ for K_z and collecting the terms multiplying K_x^2, $K_x K_y$, and K_y^2. The result of these manipulations gives the desired expressions:

$$A = [\hat{C}_{11} + \hat{C}_{33} \tan^2\theta \cos^2\varphi - 2\hat{C}_{13} \tan\theta \cos\varphi] \tag{3a}$$

$$B = 2[\hat{C}_{12} + \hat{C}_{33} \tan^2\theta \sin\varphi \cos\varphi - \tan\theta\ (\hat{C}_{13} \sin\varphi + \hat{C}_{23} \cos\varphi)] \tag{3b}$$

$$C = [\hat{C}_{22} + \hat{C}_{33} \tan^2\theta \sin^2\varphi - 2\hat{C}_{23} \tan\theta \sin\varphi] \quad . \tag{3c}$$

We note that if a = b = 1 (isotropic irregularities), then

$$A = 1 + \tan^2\theta \cos^2\varphi \tag{4a}$$

$$B = 2 \tan^2\theta \sin\varphi \cos\varphi \tag{4b}$$

$$C = 1 + \tan^2\theta \sin^2\varphi \quad . \tag{4c}$$

Thus, the diffraction pattern is not, in general, isotropic, even if the irregularities themselves are isotropic.

In most analysis [e.g., Briggs and Parkin (1963), Singleton (1973), Rufenach (1975)] a coordinate system with the z axis along the line of sight is used. As discussed in Rino and Fremouw (1977), this does not immediately give the full three-dimensional structure of the wavefield. In any case, the appropriate coefficients for the "Briggs-Parkin" system are

$$A' = [A \cos^2\varphi + B \cos\varphi \sin\varphi + C \sin^2\varphi] \cos^2\theta \tag{5a}$$

$$B' = [B \cos 2\varphi + (C - A) \sin^2\varphi] \cos\theta \tag{5b}$$

$$C' = [A \sin^2\varphi - B \sin\varphi \cos^{\varphi} + C \cos^2\varphi] \tag{5c}$$

If Eqs. (4a), (4b), and (4c) are substituted into Eqs. (5a), (5b), and (5c), it follows that $A = C = 1$ and $B = 0$. Thus, the diffraction pattern for isotropic irregularities is isotropic in a plane normal to propagation direction. This can, of course, be deduced by symmetry arguments.

DISTRIBUTION LIST

DEPARTMENT OF DEFENSE

Assistant Secretary of Defense
Comm, Cmd, Cont & Intell
ATTN: C3IST&CCS, M. Epstein
ATTN: Dir of Intelligence Systems, J. Babcock

Assistant to Secretary of Defense
Atomic Energy
ATTN: Executive Assistant

Defense Advanced Rsch Proj Agency
ATTN: TIO

Defense Communications Agency
ATTN: Code 101B
ATTN: Code 205
ATTN: Code 480, F. Dieter

Defense Communications Engineer Center
ATTN: Code R410, R. Craighill
ATTN: Code R123

Defense Nuclear Agency
(4) ATTN: TITL
(3) ATTN: RAAF

Defense Technical Information Center
(12) ATTN: DD

Field Command
Defense Nuclear Agency
ATTN: FCPR

Field Command
Defense Nuclear Agency
Livermore Division
ATTN: FCPRL

Interservice Nuclear Weapons School
ATTN: TTV

Joint Chiefs of Staff
ATTN: C3S Evaluation Office

Under Secy of Def for Rsch & Engrg
Department of Defense
ATTN: Strategic & Space Systems (OS)

WWMCCS System Engineering Org
ATTN: R. Crawford

DEPARTMENT OF ARMY

Atmospheric Sciences Laboratory
U.S. Army Electronics R & D Command
ATTN: DELAS-EO, F. Niles

BMD Advanced Technology Center
Department of the Army
ATTN: ATC-T, M. Capps
ATTN: ATC-R, D. Russ
ATTN: ATC-O, W. Davies

DEPARTMENT OF ARMY (Continued)

BMD Systems Command
Department of the Army
ATTN: BMDSC-HW

Harry Diamond Laboratories
Department of the Army
ATTN: DELHD-N-P
ATTN: DELHD-N-P, F. Wimenitz
ATTN: DELHD-I-TL, M. Weiner

U.S. Army Materiel Dev & Readiness Cmd
ATTN: DRCLDC, J. Bender

U.S. Army Missile Intelligence Agency
ATTN: J. Gamble

U.S. Army Nuclear & Chemical Agency
ATTN: Library

U.S. Army Satellite Comm Agency
ATTN: Document Control

U.S. Army Tradoc Systems Analysis Activity
ATTN: ATAA-PL

DEPARTMENT OF NAVY

Naval Electronic Systems Command
ATTN: PME-117-20
ATTN: Code 501A
ATTN: PME-117-211, B. Kruger
ATTN: PME-117-2013, G. Burnhart

Naval Research Laboratory
ATTN: Code 4780, S. Ossakow
ATTN: Code 4700, T. Coffey

Naval Surface Weapons Center
ATTN: Code F31

Office of Naval Research
ATTN: Code 465

Strategic Systems Project Office
Department of the Navy
ATTN: NSP-43
ATTN: NSP-2722, F. Wimberly

DEPARTMENT OF THE AIR FORCE

Air Force Geophysics Laboratory
ATTN: OPR, A. Stair
ATTN: OPR, H. Gardiner
ATTN: PHI, J. Buchau
ATTN: PHP, J. Mullen

Air Force Weapons Laboratory
Air Force Systems Command
ATTN: DYC
ATTN: SUL

Air Force Wright Aeronautical Laboratories
ATTN: AAD, W. Hunt
ATTN: A. Johnson

DEPARTMENT OF THE AIR FORCE (Continued)

Ballistic Missile Office
Air Force Systems Command
ATTN: MNNH, M. Baran

Deputy Chief of Staff
Research, Development, & Acq
Department of the Air Force
ATTN: AFRDQ

Headquarters Space Division
Air Force Systems Command
ATTN: SKA, M. Clavin
ATTN: SZJ
ATTN: SZJ, W. Mercer
ATTN: YA, E. Butt

Strategic Air Command
Department of the Air Force
ATTN: XPFS
ATTN: NRT

OTHER GOVERNMENT

Institute for Telecommunications Sciences
National Telecommunications & Info Admin
ATTN: W. Utlaut

DEPARTMENT OF ENERGY CONTRACTORS

Lawrence Livermore Laboratory
ATTN: L-31, R. Hager
ATTN: L-389, R. Ott

Los Alamos Scientific Laboratory
ATTN: E. Jones
ATTN: D. Simons
ATTN: MS 664, J. Zinn
ATTN: MS 670, J. Hopkins

Sandia National Laboratories
ATTN: Org 1250, W. Brown
ATTN: Org 4241, T. Wright

DEPARTMENT OF DEFENSE CONTRACTORS

Aerospace Corp.
ATTN: D. Olsen
ATTN: N. Stockwell
ATTN: V. Josephson

APTEK
ATTN: T. Meagher

Berkeley Research Associates, Inc.
ATTN: J. Workman

Charles Stark Draper Lab, Inc.
ATTN: D. Cox
ATTN: J. Gilmore

EG&G, Inc.
ATTN: D. Wright
ATTN: J. Colvin

DEPAPTMENT OF DEFENSE CONTRACTORS (Continued)

ESL, Inc.
ATTN: J. Marshall

General Electric Co.
Space Division
ATTN: A. Harcar
ATTN: M. Bortner

General Electric Co.-TEMPO
ATTN: W. McNamara
ATTN: W. Knapp
ATTN: M. Stanton
ATTN: T. Stevens
ATTN: DASIAC

General Research Corp.
ATTN: J. Ise, Jr.
ATTN: J. Garbarino

GTE Sylvania, Inc.
ATTN: M. Cross

HSS, Inc.
ATTN: D. Hansen

Institute for Defense Analyses
ATTN: E. Bauer

JAYCOR
ATTN: S. Goldman

Johns Hopkins University
Applied Physics Lab
ATTN: T. Potemra

Lockheed Missiles & Space Co., Inc.
ATTN: D. Churchill

M.I.T. Lincoln Lab
ATTN: D. Towle

Martin Marietta Corp.
ATTN: R. Heffner

McDonnell Douglas Corp.
ATTN: R. Halprin
ATTN: W. Olson
ATTN: G. Mroz

Meteor Communications Consultants
ATTN: R. Leader

Mission Research Corp.
ATTN: R. Hendrick
ATTN: R. Kilb
ATTN: D. Sappenfield
ATTN: S. Gutsche
ATTN: D. Sowle
ATTN: F. Fajen
ATTN: R. Bogusch

Mitre Corp.
ATTN: B. Adams

DEPARTMENT OF DEFENSE CONTRACTORS (Continued)

Mitre Corp.
ATTN: W. Hall
ATTN: W. Foster
ATTN: J. Wheeler

Pacific-Sierra Research Corp.
ATTN: F. Thomas
ATTN: E. Field

Photometrics, Inc.
ATTN: I. Kofsky

Physical Dynamics, Inc.
ATTN: E. Fremouw

R & D Associates
ATTN: W. Karzas
ATTN: R. Lelevier
ATTN: B. Gabbard
ATTN: C. MacDonald
ATTN: F. Gilmore
ATTN: P. Haas

R & D Associates
ATTN: B. Yoon

Rand Corp.
ATTN: C. Crain
ATTN: E. Bedrozian

DEPARTMENT OF DEFENSE CONTRACTORS (Continued)

Science Applications, Inc.
ATTN: D. Hamlin
ATTN: J. McDougall
ATTN: L. Linson
ATTN: D. Sachs

Science Applications, Inc.
ATTN: J. Cockayne

SRI International
ATTN: W. Jaye
ATTN: G. Smith
ATTN: W. Chesnut
ATTN: R. Leadabrand
ATTN: C. Rino
ATTN: M. Baron

Technology International Corp.
ATTN: W. Boquist

Teledyne Brown Engineering
ATTN: R. Deliberis

TRW Defense & Space Sys Group
ATTN: R. Plebuch

Visidyne, Inc.
ATTN: J. Carpenter
ATTN: C. Humphrey